

Synthesis and Characterization of a Novel Dapsone-Derived Bisazo Ligand and Its Gold(III) Complex, with Evaluation of Its Antioxidant and Anticancer Activities

Haider Muhammed Hessoon and Hussam Muhammed Abbas*

Department of Chemistry, College of Science, University of Al-Qadisiyah, Al-Diwaniyah 58002, Iraq

* Corresponding author:

email: sci.chem.mas.21.5@qu.edu.iq

Received: September 19, 2023

Accepted: November 4, 2023

DOI: 10.22146/ijc.89115

Abstract: In this study, we successfully synthesized a novel bisazo ligand derived from dapsone and explored its potential as a versatile coordination compound. Furthermore, we formed an Au(III) complex with this bisazo ligand and extensively characterized it using a range of analytical techniques, including UV-visible, FTIR, NMR spectroscopy, mass spectrometry, X-ray diffraction, and thermal analysis (TGA). The Au(III) complex exhibited significant inhibitory effects on liver cancer cells (HEPG2), achieving a maximum inhibition rate of 56.45% at a concentration of 400 $\mu\text{g mL}^{-1}$. Interestingly, the complex showed comparatively milder effects on normal cells (HDFn). Both the ligand and the gold complex demonstrated antioxidant properties, with ascorbic acid serving as a reference for comparison. These findings underscore the promising potential of the synthesized bisazo ligand and its Au(III) complex in medicinal chemistry, particularly for cancer treatment and antioxidant applications. Additionally, these compounds exhibit nanoscale characteristics, further enhancing their relevance in various scientific and technological fields.

Keywords: dapsone; gold; liver cancer cells; anticancer; antioxidant

■ INTRODUCTION

The field of coordination chemistry has experienced significant advancements in recent years, driven by the pursuit of designing innovative ligands and metal complexes for various applications, particularly in the realm of medicinal chemistry [1-2]. This endeavor is motivated by the profound impact that coordination compounds can exert on biological systems, establishing them as a pivotal area of research in the quest for novel therapeutic agents. In this context, our study is propelled by the aspiration to contribute to this evolving field by investigating the synthesis and characteristics of a distinctive bisazo ligand derived from dapsone and its subsequent coordination with Au(III) ions [3-4].

The development of ligands containing azo functionalities has garnered substantial interest within the coordination chemistry community. Azo compounds exhibit a rich chemistry marked by the presence of azo ($-\text{N}=\text{N}-$) groups, which can engage in diverse coordination modes, rendering them versatile candidates for coordination with metal ions [5]. Moreover, the potential

biological activities associated with azo compounds have added an intriguing dimension to their exploration in the realm of medicinal chemistry [6]. Our motivation here lies in the potential discovery of ligands with enhanced biological activities, which can serve as foundational elements for the creation of novel therapeutic agents.

Bisazo compounds, distinguished by the presence of two azo groups in their structure, have demonstrated a wide range of applications in the pharmaceutical and medical sectors [7]. These applications encompass, but are not limited to, their utilization as drug candidates, biologically active molecules, and cellular staining agents, facilitating the visualization of cellular components and metabolic processes [8-11]. Comprehending the synthesis and coordination chemistry of bisazo ligands, such as the one derived from dapsone, can open new avenues for the development of biologically active compounds and therapeutic agents.

Dapsone, a well-established compound renowned for its anti-inflammatory and antimicrobial properties,

possesses a promising structural framework comprising amino groups and an aromatic ring system. This structural foundation renders dapsone an appealing starting point for the synthesis of azo ligands. The conversion of dapsone into azo compounds introduces additional functionalities, such as electron-rich aromatic rings and azo linkages, which have the potential to augment their biological activities [12-16].

In this context, our study aims to bridge the gap between coordination chemistry and medicinal applications by presenting the synthesis and comprehensive characterization of a novel bisazo ligand derived from dapsone. The primary objective is to explore the coordination chemistry of this ligand with Au(III) ions, potentially resulting in the formation of a Au(III) complex. Au(III) complexes have gained prominence in medicinal chemistry due to their distinctive electronic and structural properties, offering a spectrum of biological activities, including anticancer and antioxidant effects [17]. By coordinating our bisazo ligand with Au(III) ions, we aspire to unveil the potential enhancement of its biological activities, thereby contributing to the development of new therapeutic agents in the rapidly advancing field of coordination chemistry in the medicinal field [18-22].

■ EXPERIMENTAL SECTION

Materials

The materials used in this study were 4,4'-diaminodiphenylsulfone (dapsone) (FERAK, 99%), sodium nitrite, (Thomas baker, 98%), sodium hydroxide (LOBA, 98%), gold(III) chloride (B.D.H., 98%), 2,4-dimethylphenol (CDH, 99%), hydrochloric acid (CGH, 38%), and dimethyl sulfoxide (LOBA, 99%).

Instrumentation

The instrumentations used in this study were Shimadzu FT-IR 8400S spectrophotometer, UV-1650 PC UV-visible spectrophotometer, Sturat digital melting point/SMP3, Bruker500 MHZ300, Agilent 5375 USA for mass spectra, and Philips X'Pert Pro diffractometer.

Procedure

Synthesis of SBDP-DMP ligand

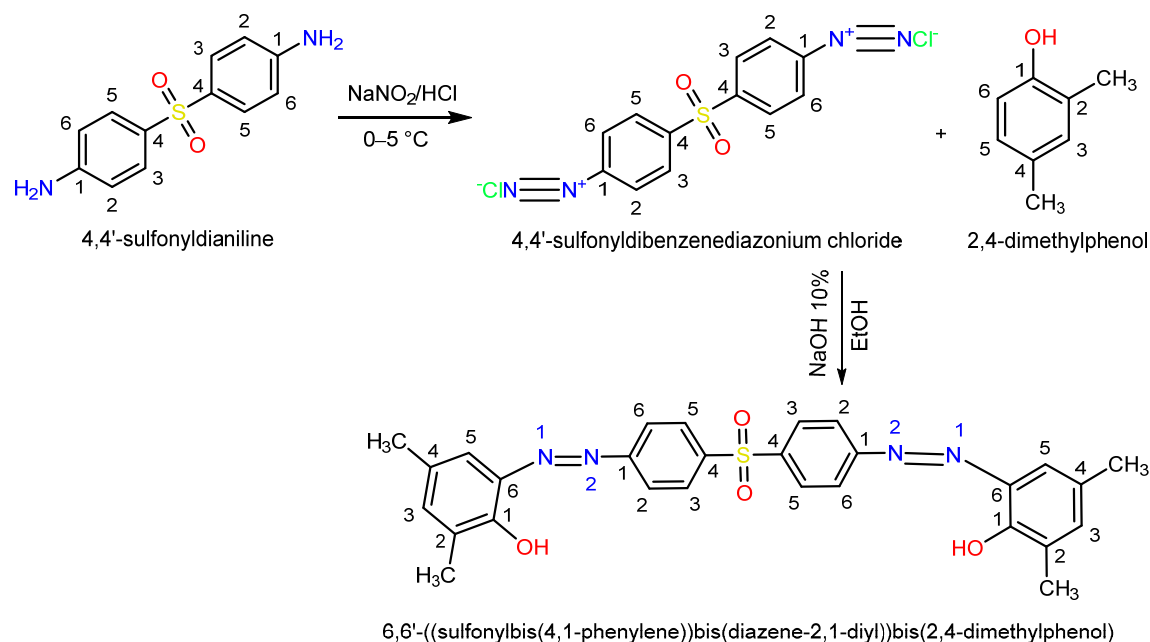
The synthesis of SBDP-DMP ligand was carried out as follows: 1.25 g (5 mmol) of 4,4'-diaminodiphenylsulfone was dissolved in a solution consisting of 5 mL of 37% hydrochloric acid and 40 mL of distilled water. The mixture was cooled to a temperature between 0 and 5 °C. Subsequently, a solution containing 0.69 g (10 mmol) of sodium nitrite in 25 mL of distilled water was added dropwise to the cooled mixture with continuous stirring, ensuring that the temperature did not exceed 5 °C. After 15 min, the diazonium solution was slowly dripped into a continuously stirred solution comprising 1.3 mL (10 mmol) of 2,4-dimethylphenol dissolved in a mixture of 17 mL of 10% NaOH and 30 mL of ethanol, completing the synthesis of ligand SBDP-DMP. Scheme 1 shows the preparation steps.

Synthesis of Au(III) complex

The Au(III) complex was synthesized in a molar ratio of 1:1 (ligand to metal). A solution of 0.339 g (1 mmol) of Au(III) chloride was prepared by dissolving it in 25 mL of ammonium acetate solution. This solution was added to a solution containing 0.257 g (1 mmol) of ligand dissolved in the same volume of absolute ethanol. The mixture was subjected to a reverse reflux process for 1 h. Subsequently, the mixture was allowed to cool, resulting in the formation of an orange precipitate. The precipitate was filtered, dried in the air, and then recrystallized by absolute ethanol to obtain the Au(III) complex in its pure form.

Free radical scavenging assessment using DPPH assay

The extracts' ability to neutralize free radicals was assessed using the DPPH radical scavenging assay. This assay measures how well the compounds donate hydrogen atoms by observing the discoloration of a DPPH solution in methanol. A 0.1 mM DPPH solution was prepared and mixed with the extracts at different concentrations (50–450 $\mu\text{g mL}^{-1}$). After 30 min in the dark at room temperature, the mixture's absorbance was



Scheme 1. Preparation steps of SBDP-DMP ligand of bisazo based on dapsone

measured at 517 nm. Ascorbic acid was used as a reference [23]. The percentage of DPPH radical scavenging activity was calculated, and IC_{50} values were determined from concentration-response curves. The experiment was repeated three times for each concentration to ensure accuracy [24-26].

Cytotoxicity assay (MTT assay)

The anticancer activity of the samples against MCF7 and H460 cells was evaluated using the 3-(4,5-dimethylthiazol-2-yl)-2,5-diphenyltetrazolium bromide (MTT) assay. Cells were seeded in 96-well plates and treated with the samples. After incubation, MTT solution was added, and the plates were further incubated to allow formazan crystal formation. Subsequently, dimethyl sulfoxide (DMSO) was used to solubilize the crystals, and the OD values were measured at 595 nm, with DMSO as a blank. Cell viability was calculated as a percentage of control, and IC_{50} values were determined by plotting a standard graph of drug concentration against relative cell viability. This assay enabled the assessment of cytotoxicity and the determination of the concentration required for 50% inhibition of cell viability [27-28].

Statistical analysis

Statistical analysis of the collected data was performed using an unpaired t-test with GraphPad Prism

software, and the results were expressed as the mean \pm standard error (SE) [29-30].

RESULTS AND DISCUSSION

The resulting ligand, known as 6,6'-((sulfonylbis(4,1-phenylene))bis(diazeno-2,1-diyl))bis(2,4-dimethylphenol), was obtained as a dark yellow powder with a product percentage of 82% and a melting point of 215 °C. This SBDP-DMP ligand is insoluble in water but completely soluble in dimethyl sulfoxide, dimethylformamide, and acetone. The synthesis involved the reaction of Au(III) with the SBDP-DMP ligand in ethanol under reflux conditions, resulting in a high-yield Au(III) complex characterized by its distinctive orange color and a melting point of 310 °C.

Mass Spectrometry

The mass spectrum of SBDP-DMP dye, as shown in Fig. 1(a), exhibited a prominent molecular ion peak at mass-to-charge ratio (m/z) 514.5. This corresponds precisely to the predicted molecular weight of the SBDP-DMP ligand. In addition, the molecular ion peak for the Au(III) complex was observed at m/z of 1048, as shown in Fig. 1(b). This m/z value aligns with the expected mass for the $[\text{Au}_2(\text{SBDP-DMP})\text{Cl}_4]$ formula of the Au(III) complex. These findings in the mass spectrum support

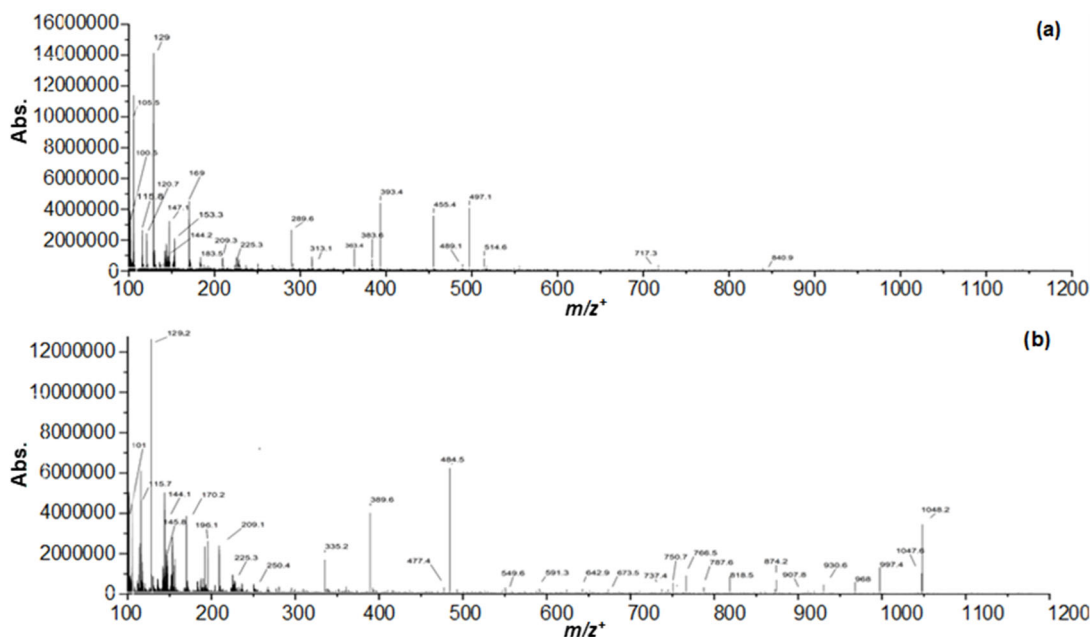


Fig 1. Mass spectrum of (a) SBDP-DMP ligand and (b) Au(III) complex for BDP-DMP ligand

Table 1. $^1\text{H-NMR}$ analysis of SBDP-DMP and $[\text{Au}_2(\text{SBDP-DMP})\text{Cl}_4]\text{H}_2\text{O}$ compounds

Proton position	SBDP-DMP		$[\text{Au}_2(\text{SBDP-DMP})\text{Cl}_4]\text{H}_2\text{O}$	
	Chemical shift (δ , ppm)	Signal type	Chemical shift (δ) (ppm)	Signal type
23, 34	11.23	Singlet (1H)	-	-
5, 15	8.21	Doublet (2H)	8.21	Doublet (2H)
11, 9	8.01	Doublet (2H)	7.96	Doublet (2H)
6, 14	7.44	Doublet (2H)	7.45	Doublet (2H)
12, 8	7.22	Doublet (2H)	7.23	Doublet (2H)
19, 30	6.66	Singlet (2H)	6.63	Doublet (2H)
32, 21	6.24	Doublet (2H)	6.13	Doublet (2H)
DMSO	2.50	Singlet	2.51	Singlet
26, 37 (Methyl)	2.62	Singlet (6H)	2.27	Singlet (6H)
25, 36 (Methyl)	2.22	Singlet (6H)	2.23	Singlet (6H)
H_2O	-	-	3.33	Singlet (2H)

the accurate determination of the molecular weights for both the ligand SBDP-DMP and the Au(III) complex, providing essential information for the characterization of these compounds [31-33].

$^1\text{H-NMR}$ Spectrum

The $^1\text{H-NMR}$ spectra of both the Au(III) complex and ligand were studied using DMSO- d_6 as the solvent and TMS as the standard reference. This was done to investigate structural changes and coordination behaviors. In the $^1\text{H-NMR}$ spectrum of the Au(III) complex, significant shifts and intensities changes were

observed in comparison to the ligand, as shown in Fig. S1 and Table 1. Notably, the absence of OH group suggests its involvement in coordination, accompanied by proton loss, leading to the formation of the studied complex [34].

Infrared Spectra

Infrared spectra for both the SBDP-DMP ligand and its Au(III) complex were obtained using KBr discs. The FTIR spectrum displayed distinct absorption bands [35-36]. The free bisazo ligand and its Au(III) complex exhibited bands at 1513 (strong) and 1475 (weak) cm^{-1} ,

respectively, attributed to the azo group ($-N=N-$). Variations were observed in the location and intensity of the bands, indicating the occurrence of coordination through this group [37]. Furthermore, weak bands related to (M–N) vibrations were detected in 456 cm^{-1} in the complexes [38], as shown in Fig. S2 and S3. Table 2 summarizes the essential vibrations of the ligand and the gold complex.

UV-vis Spectra of SBDP-DMP Ligand and Au(III) Complex

Electronic transition measurements were carried out in DMSO at room temperature [39-40]. The UV-vis spectra of the SBDP-DMP ligand and the Au(III) complex are presented in Fig. S4(a). The SBDP-DMP ligand displayed absorption bands at 259 and 385 nm. These bands are attributed to $\pi \rightarrow \pi^*$ and $n \rightarrow \pi^*$ transitions, respectively [41]. The UV-vis spectrum of the Au(III) complex exhibited a distinct absorption band at 489 nm, corresponding to the ($^1A_{1g}$) \rightarrow ($^1T_{2g}$) electronic transition as shown in Fig. S4(b). This absorption band aligns well with the expected square planar geometry of the Au(III) ion [42].

X-ray Diffraction

X-ray diffraction (XRD) analysis was conducted on the samples using an X-ray diffractometer in a controlled laboratory environment [43-44]. The obtained results revealed the presence of distinct peaks distributed along the 2θ angle axis, which signifies the angle at which X-rays

deflect upon interacting with the sample. To extract quantitative information from these results, specialized data processing software, specifically Excel, was employed for in-depth analysis. Notably, the size of the crystals was calculated using the Scherrer equation [45], which is a well-established method for determining crystallite size from XRD data. The calculations revealed that both the ligand SBDP-BN and the Au(III) complex exhibited nanoscale characteristics, with the ligand averaging a size of 14.88 nm and the Au(III) complex measuring at an average size of 35.17 nm as shown in Fig. S5 and S6. These findings underscore the nanostructured attributes of these compounds and suggest their potential utility across diverse technological and scientific domains that harness the distinctive properties of nanomaterials [46]. Table 3 presents details on the structural properties of crystalline materials, including lattice strain, crystallite size, relative intensity, height, d -spacing, FWHM, position, and compound identity. These parameters offer insights into crystallographic characteristics: strain indicates internal stress, crystallite size reveals individual sizes, and other values describe aspects like peak intensity, spacing, and compound identification.

Thermal Analysis of Au(III) Complex

The thermal degradation behavior of Au(III) complexes was investigated through TG analysis. The analysis was conducted under a nitrogen atmosphere (20 mL/min) over a temperature range of 20 to 700 °C,

Table 2. The essential vibrations of SBDP-DMP ligand and its Au(III) complex

Group	$\nu(\text{OH})$	$\nu(\text{C-H})$	$\nu(\text{C=C})$	$\nu(\text{N=N})$	$\nu(\text{S=O})$	$\nu(\text{C-O})$	$\nu(\text{C-N})$	$\nu(\text{M-O})$	$\nu(\text{M-N})$
SBDP-DMP	3404	2925	1593	1513	1270	1196	1103	-	-
Au(III)	3428	2787	1593	1475	1270	1196	1102	567	456

Table 3. XRD measurement results for SBDP-DMP and Au(III) complex

Compound	Pos. [2θ (deg)]	FWHM left [2θ (deg)]	d -spacing	Height [cts]	Rel. int. [%]	Crystallite size (nm)	Avg. D (nm)	Lattice strain
SBDP-DMP	25.154	0.590	3.540	213.910	100	13.130	14.880	0.011
	12.990	0.688	6.814	192.440	89.960	11.460		
	13.860	0.393	6.386	118.00	55.160	20.040		0.014
	13.090	0.246	6.761	440.310	100	32.080		0.009
Au(III) complex	38.309	0.344	2.349	440.280	99.990	21.790	35.170	0.004
	32.761	0.147	2.733	175.110	39.770	51.640		0.002

employing a heating rate of $20\text{ }^{\circ}\text{C min}^{-1}$. The thermal degradation behavior of the gold complex reveals a multi-step process marked by distinct mass loss events. In the initial stage ($31.11\text{--}77.69\text{ }^{\circ}\text{C}$), a minor 3.90% mass loss occurs, likely attributed to the removal of volatile components or the release of adsorbed solvents. The subsequent stages exhibit more substantial mass losses: the second stage ($77.69\text{--}251.55\text{ }^{\circ}\text{C}$) involves an 18.45% mass loss, indicating significant chemical transformations or bond cleavage; the third stage ($251.55\text{--}466.04\text{ }^{\circ}\text{C}$) continues with a 20.01% mass loss, suggesting further complex decomposition reactions; and finally, the fourth stage ($466.04\text{--}670.63\text{ }^{\circ}\text{C}$) displays a substantial 36.22% mass loss, signifying extensive decomposition. A residue remains below $670.63\text{ }^{\circ}\text{C}$. These findings underscore the intricate thermal behavior of the Au(III) complex, necessitating further investigation to elucidate the specific compounds and reactions involved in each decomposition step. The resulting thermal stability data are presented in Table 4, and a representative TGA and DTG diagram is illustrated in Fig. 2.

Molecular Geometry for the SBDP-DMP Ligand and Its Au(III) Complex

The molecular geometry of the SBDP-DMP ligand and its corresponding Au(III) complex was determined using the Avogadro computer program, a versatile tool for chemical compound editing and visualization. The optimization of molecular geometry was achieved through the Universal Force Field (UFF) method [47], a molecular mechanics-based approach that aims to minimize potential energy and attain the most energetically stable conformation. Fig. 3 and 4 show the most stable molecular geometry. The characterization

process involved various diagnostic measurements, including molar ratios, magnetic studies, and molar electrical conductivity assessments, along with analytical techniques such as $^1\text{H-NMR}$, $^{13}\text{C-NMR}$, mass spectrometry, UV-vis, infrared spectroscopy, and TG analysis. Collectively, these analyses provided valuable insights into the coordination behavior of the SBDP-DMP ligand.

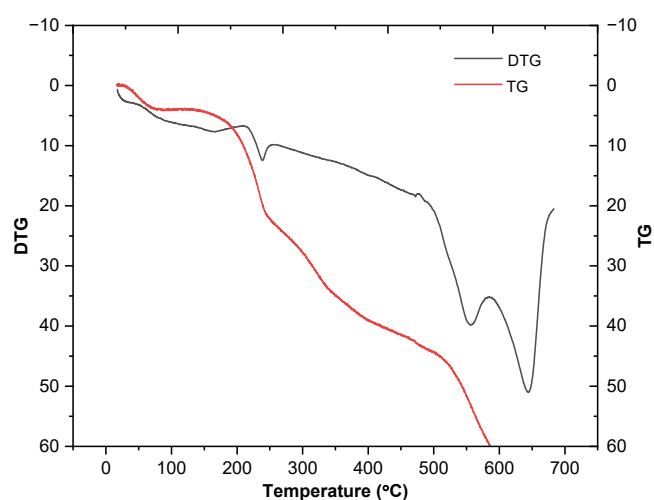


Fig 2. TGA-DTG curves of Au(III) complex

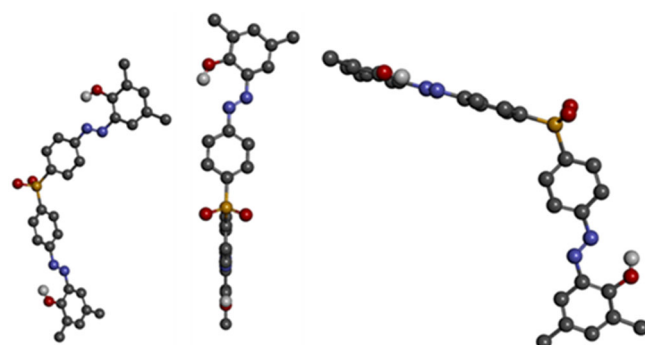


Fig 3. The lowest energy molecular geometry for ligand SBDP-DMP

Table 4. Thermal analyses data for (TGA, DTG) of Au(III) complex

Compound	Decomposition	TG range ($^{\circ}\text{C}$)	% Mass loss	% Total mass loss	DTA ($^{\circ}\text{C}$)		Metallic residue
					Nature of peaks	T_{max}	
Au(III) complex	1 st	31.11–77.69	3.90	78.58	+	236.84	$1/2\text{Au}_2\text{O}_3$
	2 nd	77.69–251.55	18.45		+	554.48	
	3 rd	251.55–466.04	20.01		+	642.41	
	4 th	466.04–670.63	36.22				
	Residue	>670.63					

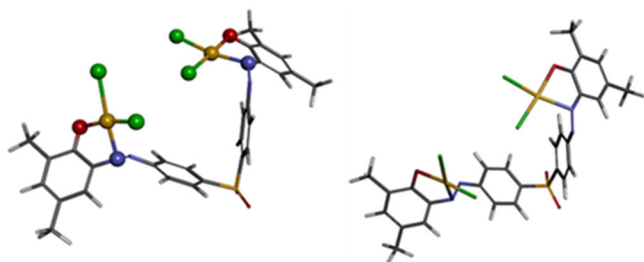


Fig 4. The lowest energy molecular geometry for a Au(III) complex

The findings suggest that the SBDP-DMP ligand exhibits a tetradentate coordination behavior, wherein coordination occurs between the distant nitrogen atoms of the azo bridge group, located at a distance from the amine ring and the oxygen atoms of the hydroxyl groups after the loss of protons. This leads to the determination of a coordination number of 4 for the Au(III) ion in the complex formed with the SBDP-DMP ligand. The proposed molecular geometry for this complex is square planar in nature (Fig. 5).

Effects of Au(III) Complex on Liver Cancer and Normal Cells

This study explores the influence of an Au(III) complex on the viability of liver cancer cells (HEPG2) and normal cells (HDFn) using MTT assay. The results reveal a concentration-dependent effect on cell survival, expressed as the percentage of remaining viable cells. Liver cancer cells displayed a range of remaining viability from 43.55 to 68.45%, while normal cells exhibited remaining viability ranging from 72.90 to 87.12%. Notably, the complex demonstrated a lower impact on HEPG2 cells at a concentration of $6.25 \mu\text{g mL}^{-1}$, with the highest reduction in viability observed at $400 \mu\text{g mL}^{-1}$ for both cell lines. Specifically, the Au(III) complex exhibited an impressive 68.45% reduction in viability for HEPG2 cells at $400 \mu\text{g mL}^{-1}$, compared to a 27.12% reduction for HDFn cells at the same concentration. Compared with previous research and studies on compounds resembling the prepared

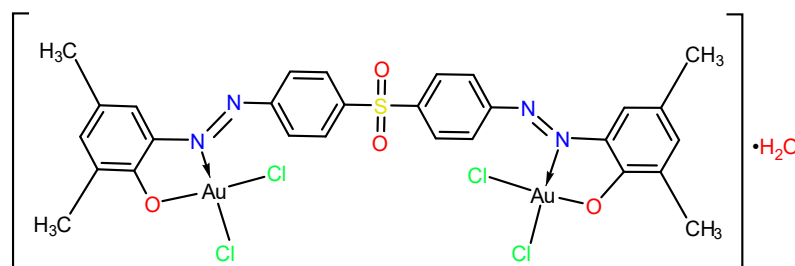


Fig 5. The proposed structural formula for the gold(III) complex with ligand SBDP-DMP

Table 5. The effect of the complex on the growth of liver cancer cells (HEPG2) and normal cells (HDFn) in different concentrations

Concentrations ($\mu\text{g mL}^{-1}$)	Au(III)-SBDP-DMP complex			
	HEPG2		HDFn	
	Mean (%)	Std. error	Mean (%)	Std. error
400	43.55	2.34	72.88	1.78
200	47.7	1.98	75.25	1.43
100	51.85	1.67	77.62	1.14
50	56	1.32	79.99	0.88
25	60.15	1.12	82.36	0.59
12.5	64.3	0.96	84.73	0.37
6.25	78.45	0.78	87.1	0.26
IC_{50} ($\mu\text{g mL}^{-1}$)	196.20		983.91	

Table 6. Antioxidant activity comparison of SBDP-DMP, Au(III) complex, and ascorbic acid using different concentrations

Compound	IC ₅₀	% inhibition				
		50 µg mL ⁻¹	150 µg mL ⁻¹	250 µg mL ⁻¹	350 µg mL ⁻¹	450 µg mL ⁻¹
SBDP-DMP	1007.74	19.89	22.52	23.76	25.8	28.98
Au(III) complex	870.70	10.41	18.23	24.39	28.54	32.66
Ascorbic acid	233.37	27.03	40.02	65.55	90.72	91.53

complex, the results are considered promising [48-49]. Table 5 illustrates the impact of the gold complex on both cells at different concentrations ranging from 6.25 to 400 µg mL⁻¹. Additionally, the table presents the value of the half-inhibitory concentration (IC₅₀).

Antioxidant Activity

The results of the DPPH assay in this study indicate that both SBDP-DMP and the Au(III) complex exhibit antioxidant properties, albeit with varying degrees of activity. Notably, the Au(III) complex demonstrates a higher level of antioxidant activity compared to SBDP-DMP. However, it is essential to emphasize that ascorbic acid, a known antioxidant, still exhibits superior antioxidant potency within the experimental context. Further research may be required to elucidate the specific mechanisms underlying the observed antioxidant effects of these compounds [50-52]. Table 6 illustrates the results of free radical scavenging analysis for compounds SBDP-DMP, Au(III) complex, and ascorbic acid, utilizing varying concentrations ranging from 50 to 450 µg mL⁻¹. Additionally, the table presents IC₅₀ of the compounds under investigation.

CONCLUSION

This study highlights the successful synthesis and characterization of a novel bisazo ligand SBDP-DMP, which was tetradentate and formed a square-planar complex with Au(III). The ligand's tetradentate nature and its subsequent square-planar coordination with the metal ion were confirmed through extensive characterization. The compounds exhibit nanoscale characteristics, highlighting their potential applications across various scientific and technological fields that leverage the unique properties of nanomaterials. The demonstrated inhibitory effects on liver cancer cells and

antioxidant properties hold promise for future research and development in the field of medicinal chemistry. Further investigations are warranted to unravel the detailed mechanisms of action and explore the full therapeutic potential of these compounds.

ACKNOWLEDGMENTS

I express my deep gratitude to the Chemistry Department at the University of Al-Qadisiyah for their invaluable support and guidance in the development of this research. This publication stands as a testament to the collaborative and scholarly environment fostered by the department.

REFERENCES

- [1] Gupta, P., Drexler, H.J., Wingad, R., Wass, D., Baráth, E., Beweries, T., and Hering-Junghans, C., 2023, P,N-type phosphalkene-based Ir(I) complexes: Synthesis, coordination chemistry, and catalytic applications, *Inorg. Chem. Front.*, 10 (8), 2285–2293.
- [2] Shanmugaraju, S., 2022, *Supramolecular Coordination Complexes: Design, Synthesis, and Applications*, Elsevier, Amsterdam, Netherlands.
- [3] Reddy, K.H., 1999, Coordination compounds in biology, *Resonance*, 4 (6), 67–77.
- [4] Adeyemi, J.O., and Onwudiwe, D.C., 2020, The mechanisms of action involving dithiocarbamate complexes in biological systems, *Inorg. Chim. Acta*, 511, 119809.
- [5] Mortadza, N.A., Ngaini, Z., and Arif, M.A.M., 2021, Synthesis of silver(I) coordination of aspirinate azo ligands as potential antibacterial agents, *Defect Diffus. Forum*, 411, 17–24.
- [6] Sahoo, J., and Paidsetty, S.K., 2016, Medicinal interest of azo-based organic compounds: A review, *Asian J. Pharm. Clin. Res.*, 9 (7), 33–39.

- [7] Shikhaliyev, N.Q., Kuznetsov, M.L., Maharramov, A.M., Gurbanov, A.V., Ahmadova, N.E., Nenajdenko, V.G., Mahmudov, K.T., and Pombeiro, A.J.L., 2019, Noncovalent interactions in the design of bis-azo dyes, *CrystEngComm*, 21 (34), 5032–5038.
- [8] Léonard, E., and Fayeulle, A., 2021, Azo-dyes-grafted oligosaccharides—From synthesis to applications, *Molecules*, 26 (11), 3063.
- [9] Bafana, A., Devi, S.S., and Chakrabarti, T., 2011, Azo dyes: Past, present and the future, *Environ. Rev.*, 19, 350–371.
- [10] Zollinger, H., 2003, *Color Chemistry: Syntheses, Properties and Applications of Organic Dyes and Pigments*, Wiley-VCH, Weinheim, Germany.
- [11] Ali, Y., Abd Hamid, S., and Rashid, U., 2018, Biomedical applications of aromatic azo compounds, *Mini-Rev. Med. Chem.*, 18 (18), 1548–1558.
- [12] Karjigi, S., Murthy, S.C., Kallappa, H., Kusuma, M.R., Aruna, B., and Reddy, Y.N., 2016, Dapsone: An update, *Indian J. Lepr.*, 87 (4), 233–239.
- [13] Wozel, G., and Blasum, C., 2014, Dapsone in dermatology and beyond, *Arch. Dermatol. Res.*, 306 (2), 103–124.
- [14] Oliveira, F.R., Pessoa, M.C., Albuquerque, R.F.V., Schalcher, T.R., and Monteiro, M.C., 2014, Clinical applications and methemoglobinemia induced by dapsone, *J. Braz. Chem. Soc.*, 25 (10), 1770–1779.
- [15] Ghaoui, N., Hanna, E., Abbas, O., Kibbi, A.G., and Kurban, M., 2020, Update on the use of dapsone in dermatology, *Int. J. Dermatol.*, 59 (7), 787–795.
- [16] Hughes, W.T., 1998, Use of dapsone in the prevention and treatment of *Pneumocystis carinii* pneumonia: A review, *Clin. Infect. Dis.*, 27 (1), 191–204.
- [17] Kyhoiesh, H.A.K., and Al-Adilee, K.J., 2023, Pt(IV) and Au(III) complexes with tridentate-benzothiazole based ligand: Synthesis, characterization, biological applications (antibacterial, antifungal, antioxidant, anticancer and molecular docking) and DFT calculation, *Inorg. Chim. Acta*, 555, 121598.
- [18] Kumar Bhaumik, P., Ghosh, K., and Chattopadhyay, S., 2021, Synthetic strategies, crystal structures and biological activities of metal complexes with the members of azole family: A review, *Polyhedron*, 200, 115093.
- [19] Manju, M., Joshi, P., and Kumar, D., 2014, Metal complexes of biological active 2-aminothiazole derived ligands, *Russ. J. Coord. Chem.*, 40 (7), 445–459.
- [20] Gassim, F.A.Z.G., and Makkawi, A.J.J., 2023, Anticancer activity of synthesized ZnO and ZnO/AgCl nanocomposites against five human cancer cells, *Indones. J. Chem.*, 23 (2), 333–340.
- [21] Irfandi, R., Raya, I., Ahmad, A., Fudholi, A., Natsir, H., Kartina, D., Karim, H., Santi, S., and Salnus, S., 2022, Review on anticancer activity of essential metal dithiocarbamate complexes, *Indones. J. Chem.*, 22 (6), 1722–1736.
- [22] Yasir, A.F., and Jamel, H.O., 2023, Synthesis of a new DPTYEAP ligand and its complexes with their assessments on physical properties, antioxidant, and biological potential to treat breast cancer, *Indones. J. Chem.*, 23 (3), 796–808.
- [23] Gęgotek, A., and Skrzydlewska, E., 2023, Ascorbic acid as antioxidant, *Vitam. Horm.*, 121, 247–270.
- [24] Rahman, M.M., Islam, M.B., Biswas, M., and Khurshid Alam, A.H.M., 2015, *In vitro* antioxidant and free radical scavenging activity of different parts of *Tabebuia pallida* growing in Bangladesh, *BMC Res. Notes*, 8 (1), 621.
- [25] Celiz, G., Renfige, M., and Finetti, M., 2020, Spectral analysis allows using the DPPH* UV–Vis assay to estimate antioxidant activity of colored compounds, *Chem. Pap.*, 74 (9), 3101–3109.
- [26] Rubab, M., Chelliah, R., and Oh, D.H., 2022, Screening for Antioxidant Activity: Diphenylpicrylhydrazine (DPPH) Assay, in *Methods in Actinobacteriology*, Eds. Dharumadurai, D., Springer US, New York, US, 453–454.
- [27] Senthilraja, P., and Kathiresan, K., 2015, *In vitro* cytotoxicity MTT assay in Vero, HepG2 and MCF-7 cell lines study of marine yeast, *J. Appl. Pharm. Sci.*, 5 (3), 80–84.
- [28] Ibrahim, A.A., Kareem, M.M., Al-Noor, T.H., Al-Muhimeed, T., AlObaid, A.A., Albukhaty, S., Sulaiman, G.M., Jabir, M., Taqi, Z.J., and Sahib,

- U.I., 2021, Pt(II)-thiocarbohydrazone complex as cytotoxic agent and apoptosis inducer in Caov-3 and HT-29 cells through the P53 and Caspase-8 pathways, *Pharmaceuticals*, 14 (6), 509.
- [29] Ali, I.H., Jabir, M.S., Al-Shmgani, H.S.A., Sulaiman, G.M., and Sadoon, A.H., 2018, Pathological and immunological study on infection with *Escherichia coli* in ale BALB/c mice, *J. Phys.: Conf. Ser.*, 1003 (1), 012009.
- [30] Jabir, M.S., Rashid, T.M., Nayef, U.M., Albukhaty, S., AlMalki, F.A., Albaqami, J., AlYamani, A.A., Taqi, Z.J., and Sulaiman, G.M., 2022, Inhibition of *Staphylococcus aureus* α -hemolysin production using nanocurcumin capped Au@ZnO nanocomposite, *Bioinorg. Chem. Appl.*, 2022, 2663812.
- [31] Pérez-Arantegui, J., and Laborda, F., 2019, Inorganic mass spectrometry, *Phys. Sci. Rev.*, 4 (3), 20180003.
- [32] Ferranti, P., and Picariello, G., 2016, "Mass Spectrometry: Applications" in *Encyclopedia of Food and Health*, Eds., Caballero, B., Finglas, P.M., and Toldrá, F., Academic Press, Oxford, UK, 654–660.
- [33] Muddiman, D.C., 2018, Jürgen H. Gross: Mass spectrometry: A textbook, 3rd ed., *Anal. Bioanal. Chem.*, 410 (8), 2051–2052.
- [34] Drew, M.G.B., Murphy, B.P., Nelson, J., and Nelson, S.M., 1987, Dicopper(II) complexes of a 28-membered N8 macrocycle. Evidence for proton transfer from co-ordinated secondary amine to thiocyanate, leading to formation of an Isothiocyanic acid complex, *J. Chem. Soc., Dalton Trans.*, (4), 873–879.
- [35] Bahjat, H.H., Ismail, R.A., Sulaiman, G.M., and Jabir, M.S., 2021, Magnetic field-assisted laser ablation of titanium dioxide nanoparticles in water for anti-bacterial applications, *J. Inorg. Organomet. Polym. Mater.*, 31 (9), 3649–3656.
- [36] Jihad, M.A., Noori, F.T.M., Jabir, M.S., Albukhaty, S., AlMalki, F.A., and Alyamani, A.A., 2021, Polyethylene glycol functionalized graphene oxide nanoparticles loaded with *Nigella sativa* extract: A smart antibacterial therapeutic drug delivery system, *Molecules*, 26 (11), 3067.
- [37] Tran, N.H., Kucharský, Š., Waring, T.M., Atmaca, S., and Beheim, B.A., 2021, Limited scope for group coordination in stylistic variations of kolam art, *Front Psychol.*, 12, 742577.
- [38] Lecoutre, M., Rohart, F., Huet, T.R., and Maki, A.G., 2000, Photoacoustic detection of new bands of HCN between 11 390 and 13 020 cm^{-1} , *J. Mol. Spectrosc.*, 203 (1), 158–164.
- [39] Jabir, M.S., Nayef, U.M., Abdulkadhim, W.K., Taqi, Z.J., Sulaiman, G.M., Sahib, U.I., Al-Shammari, A.M., Wu, Y.J., El-Shazly, M., and Su, C.C., 2021, Fe₃O₄ Nanoparticles capped with PEG induce apoptosis in breast cancer AMJ13 cells via mitochondrial damage and reduction of NF- κ B translocation, *J. Inorg. Organomet. Polym. Mater.*, 31 (3), 1241–1259.
- [40] Khashan, K.S., Abdulameer, F.A., Jabir, M.S., Hadi, A.A., and Sulaiman, G.M., 2020, Anticancer activity and toxicity of carbon nanoparticles produced by pulsed laser ablation of graphite in water, *Adv. Nat. Sci: Nanosci. Nanotechnol.*, 11 (3), 035010.
- [41] Mikheev, Y.A., and Ershov, Y.A., 2018, Assignment of the $\pi \rightarrow \pi^*$ and $n \rightarrow \pi^*$ transitions to the spectral bands of azobenzene and dimethylaminoazobenzene, *Russ. J. Phys. Chem. A*, 92 (8), 1499–1507.
- [42] Grebenkin, S.Y., Syutkin, V.M., and Baranov, D.S., 2017, Mutual orientation of the $n \rightarrow \pi^*$ and $\pi \rightarrow \pi^*$ transition dipole moments in azo compounds: Determination by light-induced optical anisotropy, *J. Photochem. Photobiol., A*, 344 (1), 1–7.
- [43] Mohammed, M.K.A., Mohammad, M.R., Jabir, M.S., and Ahmed, D.S., 2020, Functionalization, characterization, and antibacterial activity of single wall and multi wall carbon nanotubes, *IOP Conf. Ser.: Mater. Sci. Eng.*, 757 (1), 012028.
- [44] Khashan, K.S., Jabir, M.S., and Abdulameer, F.A., 2018, Preparation and characterization of copper oxide nanoparticles decorated carbon nanoparticles using laser ablation in liquid, *J. Phys.: Conf. Ser.*, 1003 (1), 012100.
- [45] Muniz, F.T.L., Miranda, M.A.R., Morilla dos Santos, C., and Sasaki, J.M., 2016, The Scherrer equation and the dynamical theory of X-ray diffraction, *Acta Crystallogr., Sect. A: Found. Crystallogr.*, 72 (3), 385–390.

- [46] Akbari, B., Tavandashti, M.P., and Zandrahimi, M., 2011, Particle size characterization of nanoparticles – A practical approach, *Iran. J. Mater. Sci. Eng.*, 8 (2), 48–56.
- [47] Jaillet, L., Artemova, S., and Redon, S., 2017, IM-UFF: Extending the universal force field for interactive molecular modeling, *J. Mol. Graphics Modell.*, 77, 350–362.
- [48] Fnfoon, D.Y., and Al-Adilee, K.J., 2023, Synthesis and spectral characterization of some metal complexes with new heterocyclic azo imidazole dye ligand and study biological activity as anticancer, *J. Mol. Struct.*, 1271, 134089.
- [49] Jasim, F.N., and Mohsein, H.F., 2022, Synthesis, identification and anticancer evaluation of new heterocyclic compounds derived from 2-benzimidazolylacetonitrile, *HIV Nurs.*, 22 (2), 1410–1415.
- [50] Hashim, M., and Fry, J., 2020, Evaluation of direct and indirect antioxidant properties of selected four natural chemical compounds: Quercetin, epigallocatechin-3-gallate, indole-3-carbinol and sulforaphane by DPPH radical scavenging assay, *J. Biomed. Res. Environ. Sci.*, 1 (8), 389–392.
- [51] Skroza, D., Šimat, V., Vrdoljak, L., Jolić, N., Skelin, A., Čagalj, M., Frleta, R., and Generalić Mekinić, I., 2022, Investigation of antioxidant synergisms and antagonisms among phenolic acids in the model matrices using FRAP and ORAC methods, *Antioxidants*, 11 (9), 1784.
- [52] Sönmez, F., Gür, T., and Şahin, Z., 2023, Thiophenyl-chalcone derivatives: Synthesis, antioxidant activity, FMO energies and molecular parameters, *Balıkesir Üniv. Fen Bilim. Enst. Derg.*, 25 (1), 293–304.